Int J Adv Manuf Technol (2002) 19:646–654

The International Journal of
Advanced
Manufacturing
Technology

Laser Based Flexible Fabrication of Functionally Graded Mould Inserts

W. Jiang and P. Molian

Department of Mechanical Engineering, Iowa State University, Ames, IA, USA

A CO_2 laser-based freeform fabrication process with emphasis on difficult-to-shape and functionally effective materials was investigated with regard to fabrication of dies and moulds. Square and circular moulds were built by use of a material additive process of layers of TiC and Ni-alloy composite. The effects of laser processing on the quality, microstructures, and hardness of the moulds were determined. Additionally, the mould performance was evaluated in die-casting, injection moulding, and in a thermal fatigue environment. The TiC core-Ni-alloy shell mould outperformed moulds made of hardened H13 die steel, 304 stainless steel, and TiC-coated stainless steel in withstanding stresses and in retaining dimensional stability at elevated temperatures.

Keywords: Casting; Die and mould; Functionally graded materials; Injection moulding; Laser processing; Thermal fatigue

1. Introduction

The global market for dies and moulds is estimated at 65 billion US dollars [1]. For die and mould makers to maintain their leading edge in this fiercely competitive market, they must use modern materials and fabrication technologies. Feasibility, cost, productivity and quality are important criteria that must be considered when methods are chosen for manufacturing moulds and dies. Conventional processing of moulds and dies typically involves multiple steps ranging from CNC machining and heat treatment to surface coating. Final shaping often relies on electrical-discharge machining (EDM) owing to the requirements of high dimensional accuracy and extremely good surface quality for moulds and dies [2]. However, EDM is a costly and time-consuming process. High on the die and mould makers' wish list are the ability to produce functional parts of good quality directly from computer geometric data (CGD) and to shorten the lead time by near-net-shape processing. Lasers have emerged as good tools in cutting, joining, and various rapid prototyping technologies [3]. Using lasers can be an efficient means of realising flexible manufacturing processes for moulds and dies because of the flexibility of integration with computers and robots. A laser-based flexible fabrication (LBFF) process could make functionally graded metallic parts with a reduction of process time. LBFF is a computer integrated, numerical-controller guided, beam-shaped laser cladding (LC) process that uses a high power CO_2 laser to melt and fully solidify powders from the base up in thin horizontal

Correspondence and offprint requests to: Professor P. Molian, Department of Mechanical Engineering, Iowa State University, 3031 HM Black Engineering Building, Ames, IA 50011–2161, USA. E-mail: molian@iastate.edu

Table 1. LC-based rapid prototyping processes.

Name	Process characteristics
Laser engineered net shaping (LENS, Sandia National Laboratory) [3]	Nd:YAD laser. Powders delivered through a concentric nozzle with laser beam. Enclosed envelop for fabrication.
Direct metal deposition (DMD, University of Michigan) [4]; Precision optical manufacturing (POM, Precision Optical Manufacturing Co. Inc)* [5]	CO_2 laser. Powders delivered through a concentric nozzle with laser beam. Height sensor control.
Laser direct casting (LDC, University of Liverpool) [5]	CO_2 laser. Powder delivered through a nozzle from one side.
Direct light fabrication (DLF, Las Alamos National Laboratory) [6,7]	Nd:YAG laser. Powder delivered through a concentric nozzle with laser beam.
Shaped deposition manufacturing (SDM, Stanford University) [8] High-power laser based fabrication process (The Pennsylvania State University) [5]; Lasform (AeroMet Corp.) [5,9]	Nd:YAG laser. CNC milling (a hybrid process). CO_2 laser. Powder delivered through a concentric nozzle with laser beam.

*The equipment is based on DMD, University of Michigan [5].

layers and to build free-standing structures. It is different from other LC-based rapid prototyping processes (Table 1) in that LBFF uses shaped laser beams that can produce layers of improved surface finish, and dimensional tolerance and reduced dilution in the functional layers. The shaped laser beam has a reduced temperature gradient in both the laser scanning direction and the transverse direction, and significantly reduced heat conduction losses; it preheats the powder at the leading edge, and facilitates even melting and a smoother flow of the molten puddle. Although studies on the fabrication of metal parts using LC-based rapid prototyping technologies have been reported [4–9], few results have been published on the use of a laser-based process to fabricate mould inserts from functionally graded materials. Die and mould inserts are generally made of hardened steels, cast irons, and superalloys. The properties required for mould and die materials are:

1. High strength.
2. High wear resistance.
3. Moderate to high toughness.
4. Low friction.
5. Chemical inertness.
6. Thermal shock resistance.
7. Corrosion resistance.

Because all these properties are seldom found in a single material, it is essential that new strategies, other than the application of a coating on the die surfaces, be developed to meet those functional requirements. This work used an approach that involved functionally graded materials (FGMs) to improve the performance and life of dies and moulds. A functionally graded material is a combination of two or more materials in which a gradual transition exists at their interface. With a gradual transition, combinations of properties on opposing surfaces can be obtained without any "weak link". Some examples of FGMs are ZrO_2/Ni-Cr, stainless steel/zirconia, and Inconel/steel [10]. In the present work, TiC/Ni-Cr-Al-Co-Y_2O_3 was selected as the combination that meets most of the property requirements. The LBFF processing, characterisation, and functional testing of FGM mould inserts were investigated in detail to demonstrate the benefits of the process and material for enhancing the performance of die-casting dies and injection moulds. Because LBFF is a material additive process, it could also be used effectively in mould and die repair, surface modification, and coatings.

2. Materials and Experimental Procedures

2.1 Material Selection

Powder materials used in making functionally graded parts, must have the desired mechanical and thermal properties. In addition, they must be thermally compatible to prevent the initiation of cracks. Based on these criteria and the application requirements for dies in die-casting and moulds in injection moulding, TiC powder with a nominal size of 2 μm and Ni-Cr-Al-Co-Y_2O_3 (Ni-alloy composite) with a nominal size of 100 μm were selected. TiC, one of most commonly used materials for coatings, has excellent physical properties. It has a thermal expansion coefficient (TEC) of 7.0×10^{-6} °C^{-1} [11] and has superior resistance to abrasive wear and corrosion when used as a coating [12,13]. Ni-alloy composite powder is a high-temperature material that has very good corrosion resistance and moderate wear resistance [14]. Its thermal expansion coefficient of 14.5×10^{-6} °C^{-1} is close to that of H13 die steel [11]. However, it has a much higher thermal conductivity than H13 die steel. The TiC was procured from Alfa Aesar® and the Ni-alloy composite powder was obtained from Sulzer Metco®. Table 2 gives the nominal composition of the Ni-alloy composite powder. AISI 304 stainless steel was used both as the supporting material and as the material for injection moulds, for comparison. Hardened H13 die steel was chosen as the base for comparison in die-casting and thermal fatigue tests, because it is widely used as the die steel in aluminium die casting. It has a hardness of 46–48 HRC after heat treatment. The temperature and time used for hardening H13 die steel are provided in Table 3.

Table 2. Nominal chemical composition of the Ni-alloy composite power.

Element	Ni	Cr	Al	Co	Y_2O_3
Weight (%)	balanced	17.5	5.5	2.5	0.5

2.2 The LBFF Process

The LBFF process uses a high-power CO_2 laser to melt the powder which is delivered by inert gas in the laser-material interaction zone and builds a rapidly solidified structure in near fully dense material and near-net-shape, layer by layer. A diagram of this process is shown in Fig. 1. It starts with a 3D solid model, which is a geometric representation of designed moulds or dies. CAD/CAM software is then used to slice the 3D model in the *Z*-direction and to transfer the 3D model into 2D "blocks" of typical thickness 0.2–0.3 mm. From these, CNC codes, such as those used in the pocket milling process, are created. The codes are then used to direct the laser beam scanning in a raster pattern within the boundaries defined by the slices. The motion of the substrate in the *X*- and *Y*-directions, in combination with the motion of the optics in the *Z*-direction, allows the generation of arbitrary 3D structures. The feedstock could be wire or powder. Wire is relatively easy to feed, but is often difficult to obtain in the required chemical composition. Powder is much easier to procure and can be fed into the interaction zone either by pre-placing it or delivering it directly. However, control of the delivery rate of

Table 3. Temperature and time used for hardening H-13 die steel.

Procedures	Stress relief	Vacuum air hardening	Tempering I	Tempering II
Temperature (°C)	537	1024	537	537
Time (h)	0.5	1.5	3	3

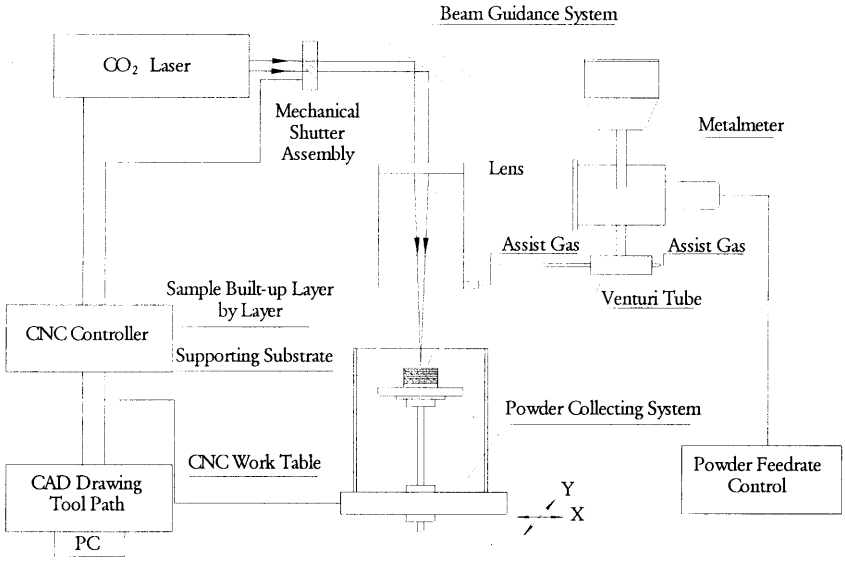

Fig. 1. The set-up for the LBFF process.

the powder is critical. Powder which is not melted by the laser beam can be collected and reused, reducing the waste material and reducing damage to the environment. A continuous wave (CW) CO_2 laser with a power output of up to 2000 W was used in this work because of its high power and its Gaussian beam profile, which can focus the beam to a small spot size.

2.2.1 Deposition of the Ni-Alloy Composite Powder

In this fabrication process, the laser beam was directed to the 304 stainless steel surface by means of a lens with a focal length of 190 mm. The beam was defocused by 6.4 mm below its focal point to avoid the laser-cutting mode. The beam diameter at the sample surface was 0.5 mm. Power density was about 4.1×10^5 W cm^{-2}, which is close to the value recommended for metal melting [15]. The Ni-alloy composite powder was transported to the interaction zone by a nozzle by argon, which was also used as a shielding gas, from the side. The deposition thickness for each Ni-alloy powder layer was approximately 0.25 mm. The powder feedrate was monitored by adjusting the powder delivery motor speed. The laser beam scanned the substrate according to the profiles and tool paths obtained by use of CAD/CAM software. Table 4 gives the laser parameters and processing variables for the process that creates layers of good surface finish and high quality.

2.2.2 Deposition of the TiC Powder

Because TiC powder readily "boils" at elevated temperatures, producing a rough surface during the deposition process, a diffused rectangular beam generated by a cylindrical–spherical lens with a focal length of 127 mm was used. The beam was focused on the substrate surface and had a spot size of 0.1 mm × 1 mm. A rectangular beam, which generates temperature gradient profiles that differ from those of a circular beam for a given power, is beneficial in forming a uniform and smooth TiC layer. The power density for this process was 5×10^5 W cm^{-2}. Because of its cubic crystal structure and fine particle size, the TiC powder was difficult to deliver through a nozzle with the existing set-up. Hence, it was placed on the substrate before being subjected to laser melting. The incremental layer thickness of TiC, 0.1 mm, was controlled by use of a weighing device with an accuracy of $\frac{1}{1000}$ g. Argon was used as a shielding gas to prevent the TiC from decarburisation. The laser parameters and processing variables for the TiC powder are given in Table 5.

Table 5. Laser parameters and processing variables for deposition of the TiC powder.

Laser power (W)	Beam geometry	Beam mode	Focal position	Scanning speed (mm s^{-1})	Stand-off distance (mm)	Assist gas flow (l s^{-1})
500	Line	TEM_{00}	Surface	50.8	2–3	0.12

Table 4. Laser parameters and processing variables for deposition of the Ni-alloy composite powder.

Laser power (W)	Beam geometry	Beam mode	Focal position	Scanning speed (mm s^{-1})	Powder feed rate (g min^{-1})	Stand-off distance (mm)	Assist gas flow (l s^{-1})	Distance between adjacent passes (mm)
800	Circle	TEM_{00}	6.4 mm below	5	17.5	13.0	0.078	0.25

2.3 Characterisation and Hardness Testing

A surface profilometer with a 0.25 mm diamond probe was used to measure the surface roughness (arithmetic average, R_a) of the fabricated parts in both the longitudinal and transverse directions. This value was then used to determine the need for post-processing. The fabricated parts were polished, etched in a solution of nitric acid, acetic acid, hydrochloric acid, and glycerin, and then examined under an optical microscope. A scanning electron microscopy (JEOL JSM35, 10 kV) was also used to characterise the profile, flaws, and microstructures of the graded layers. Parts were evaluated by means of Vickers microhardness test with a diamond pyramid indenter at a load of 1 kgf.

2.4 CNC Machining

A CNC mill was used to remove the supporting material (304 stainless steel) from the fabricated parts and to cut pockets on as-received 304 stainless steel, hardened H13 die steel, so that the moulds could be used for casting and injection moulding tests. Because of the high hardness at the interface between the 304 stainless steel support and the fabricated layers, carbide-milling bits and CAP® magic cutting fluids were used. All parts were cut using the same cutting parameters.

2.5 Functional Testing

2.5.1 Die Casting of Aluminium Alloy

Shell moulds cut from the fabricated FGM (Ni-Cr-Al-Co-Y_2O_3+TiC), laser coated 304 stainless steel (TiC as coating), as-received 304 stainless steel, and the hardened H13 die steel blocks were used as dies for pouring 319 aluminium alloy. More than 100 castings with pouring temperatures above 1033 K were produced in the dies.

2.5.2 Injection Moulding

FGM and the laser-coated, as-received 304 stainless steel mould inserts of zero taper angle were used for injection moulding to determine the mould relief ability, the presence of macro-defects, and the ability to resist stress deformation. A Boy 30M injection moulder was used for the injection process. Polystyrene was the injection material. The inserts were so configured that each insert was the same distance from the sprue hole, to negate the effect of pressure differences with distance, on stress deformation (Fig. 2). Moreover, the bottoms of the inserts were supported only on their edges so that deformation could be produced under injection pressure. The wall thickness was 1 mm for all three inserts. A Brown & Sharpe coordinate measurement machine (CMM) was then used to measure the extent of deformation. Injections were restricted to 25, owing to the difficulty in removing the injected blocks from the inserts. The injection temperature and pressure were set to 210°C and 100 bars, respectively.

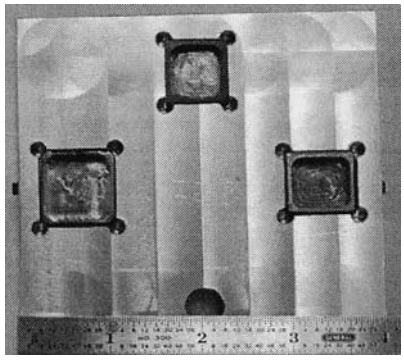

Fig. 2. The configuration of mould inserts for the injection moulding processes.

2.5.3 Low-Cycle Thermal Stress Fatigue Tests

Thermal fatigue tests on the FGM mould insert, the laser-coated 304 stainless steel and the hardened H13 tool steel mould inserts, were performed by alternately immersing them into a heated furnace for a preset time and then dropping them into a water sink. The furnace was set to temperatures of approximately 650°C and 960°C. All the mould inserts had the same geometry and were tested under the same conditions. Before being tested, the inserts were visually examined for any cracks by use of a microscope with ×20 magnification. The inserts were then checked for crack initiation with cycle intervals of 5, 10, 15, 20, 25, 35, and 50. The cycle at which crack initiation occurred was the governing criterion for thermal fatigue.

3. Results and Discussion

3.1 Analysis of Moulds Fabricated with Ni-Alloy Composite Powder

Figure 3 shows a circular mould and a square mould fabricated by use of the LBFF process in 10 and 15 passes, respectively. The circular mould has a diameter (D) of 25.4 mm. The square mould has a side length (L) of 19 mm. Both have a wall thickness of 1.2~1.5 mm. The wall thickness, which is affected by beam diameter, laser power, and pressure of shielding gas, can vary from about 1.0 mm to 3.0 mm in the LBFF process. The ratio of height to width for a single pass is about 0.2, which results in good bonding and minimum dilution. The

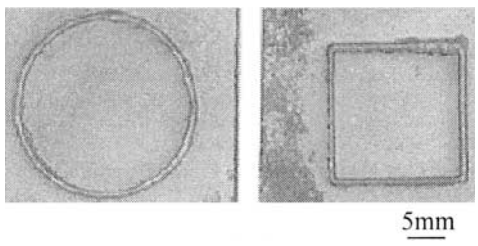

Fig. 3. Circular ($D = 25.4$ mm, $h = 2.4$ mm) and square ($L = 19.0$ mm, $h = 3.5$ mm) moulds made by LBFF (laser power = 800 W, speed = 5 mm s^{-1}).

surface roughness (R_a value) is about 200 μm. Visual examination revealed some partially melted powder particles "suspended" on the walls; the thickness was greater at the beginning and end regions of the laser irradiation than elsewhere. The partially melted particles result in the rough surfaces and possibly the non-uniformity of the wall thickness of the parts as well. The thickness build-up could be remedied by leaving a gap half as wide as the scanning width between the starting and end point [16]. A post surface finishing process is recommended for the LBFF process. Optical microscopy did not reveal any porosity and confirmed the production of near fully dense parts.

3.2 Analysis of Layers Fabricated with TiC Powder

The crucial aspect of deposition of TiC powder is its surface roughness, which greatly affects the later addition of the Ni-alloy composite powder layer. If the surface roughness of the built TiC layer exceeds 50 μm, the added Ni-alloy composite powder layer will create significant surface waviness. For powder processing, the surface roughness of one layer could be propagated to another layer and even amplified [10]. Experiments indicated that thin layers of TiC powder (<0.1 mm) built up each time, produced a smooth surface. Surface roughness (R_a value) measurements on the TiC layer along the longitudinal and the transverse directions did not differ significantly. The built-up layers had a surface roughness of less than 20 μm. Optical microscopy results showed that the built TiC layer was fully melted and there were only minor inclusions in the solidified layer (Fig. 4). Scanning electron microscopy (SEM) analysis revealed the presence of some microcracks in the layer (Fig. 5). The microcracks could have been produced by stresses during the rapid cooling that followed solidification. Crack initiation sites could be reduced or even eliminated by improved processing together with use of fine and spheroidised carbide particles [17]. Vickers microhardness measurements on the deposited layer showed an average hardness value of 1475 HV, almost 20% higher than the reported microhardness value for TiC layers. The increase in hardness may be explained by TiC particle size differences and the possible formation of titanium nitride during the deposition process. The layers exhibited a light golden colour which is characteristic of TiN.

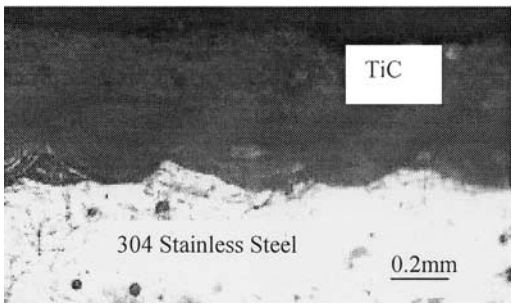

Fig. 4. Optical microscopy showing the transverse section of the fully melted TiC layer (thickness = 0.5 mm).

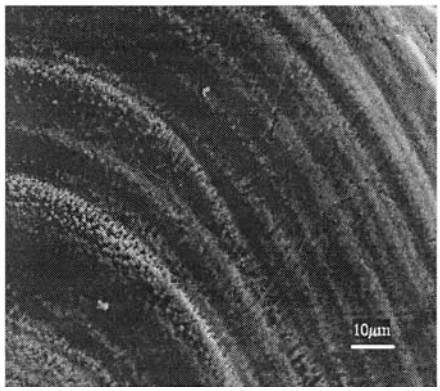

Fig. 5. SEM showing the microcracks and solidification fronts (×1000) in the TiC layer.

3.3 Analysis of Block Fabricated with Ni-Alloy Composite Powder Layer onto TiC Powder Layer

Figure 6 shows the fabricated FGM block of multiple layers, the outer layers are of Ni-Cr-Al-Co-Y_2O_3 and the inner layers are of TiC. Four passes per side produced a layer thickness of approximately 1 mm. Some inclusions in the fabricated layers were observed. The surface roughness (average value, R_a) was 10 μm. A difference of approximately 25% existed between the R_a values for the laser beam scanning direction and those for the perpendicular direction, owing to front solidification effects. Optical microscopy indicated good bonding between the TiC powder layer and the Ni-alloy powder layer. A higher power and lower scanning speed were used for the deposition of Ni-alloy composite powder than for the deposition of TiC powder. Re-melting of some TiC due to the deposition of Ni-alloy composite powder eliminated the inclusions observed in TiC (Fig. 7). The SEM showed that dendrite structures were present in both Ni-alloy and TiC layers. In the Ni-alloy layer, the dendrites were well formed and oriented (Fig. 8), which indicated that cooling of the molten pool had proceeded non-uniformly. The dendrites in the TiC layer were not fully developed (Fig. 9). The average arm spacing between secondary dendrites in the TiC layer is about 3.5 μm, while spacing for the Ni-alloy composite layer is 7.0 μm. Based on the secondary dendrite arm spacing, the cooling rates for the Ni-alloy layer and TiC layer are found to be of the order of 10^2 K s^{-1} ~ 10^3 K s^{-1}. These cooling rates are high in compari-

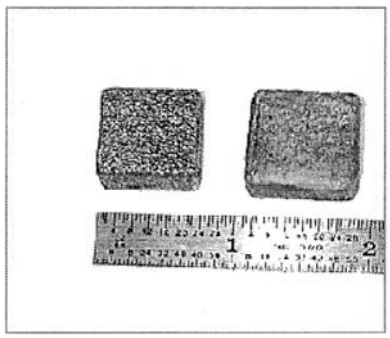

Fig. 6. Photographs of the fabricated blocks by LBFF.

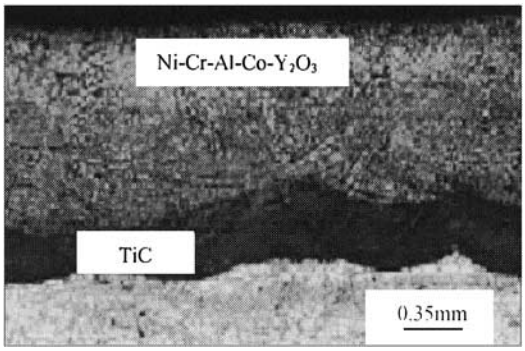

Fig. 7. Optical micrograph showing the structure of the layers of TiC and Ni-alloy.

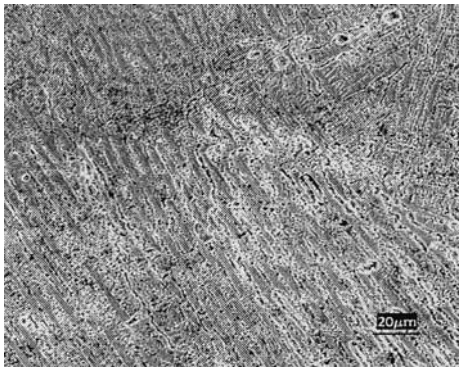

Fig. 8. SEM showing the formation of dentrites in the Ni-alloy layer.

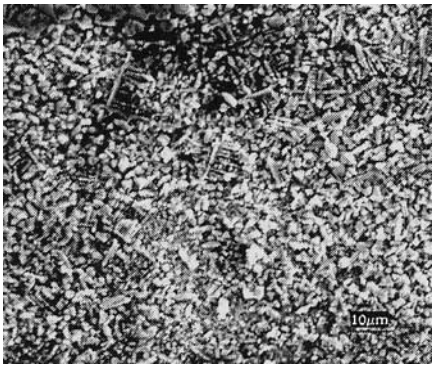

Fig. 9. SEM micrograph showing the formation of dendrites in the TiC layer.

son with the cooling rates obtained by conventional methods, but they are typical of the laser material processing.

Figure 10 shows Vickers microhardness values vary with the distance from the FGM block surface. The Ni-alloy layer had an average hardness value of 583 HV, which was close to the hardness of the hardened H13 die steel, while the TiC layer had an average hardness value of only 260 HV, almost the same as that of the supporting material. The average microhardness value in the interface region was between that of the two layers. This type of hardness profile is desired for most mould parts, especially for mould cores, because high surface hardness and acceptable toughness are desired mechanical properties. The large reduction in microhardness of the TiC layer in the FGM part was attributed to its decarburisation during the re-melting process, during the deposition of the Ni-alloy layer. This conclusion was based on the elemental analysis of energy by the energy dispersive spectrum (EDS), which indicated diffusion of carbon into the Ni-alloy layer from the TiC layer (Fig. 11).

3.4 Performance Evaluation

The performance of the mould inserts was evaluated in die-casting, injection moulding, and a low-cycle thermal fatigue environment. For the purpose of discussion, all the mould inserts are classified as shown in Table 6. Their surface roughness (R_a value) and surface microhardness (Vickers, with a load of 1 kg) are also given in the table. The FGM mould insert has a microhardness close to hardened H13 die steel, however, it has a much rougher surface, indicating the necessity of some post-processing.

3.4.1 319 Aluminium Alloy Casting

Inserts B, C, and D were used as shell moulds for aluminium alloy casting. Over a hundred 319 aluminium alloy blocks were cast. There was no difficulty in removing the castings from the moulds, although the cavities had zero draft angles. There were no significant differences among the cast 319 aluminium alloy blocks poured into these moulds. Repeated expansion and contraction during the casting process owing to thermal cycles did not cause the cavities to deteriorate, suggesting that a more severe test was required for comparison purposes. This test was intended as a functionality check rather than as a means of comparison between parts.

3.4.2 Injection Moulding

An injection moulding test to examine the ease of mould relief and the ability of the insert to withstand stress deformation was performed on mould inserts A, C, and D. Test showed that the injected polystyrene blocks were not easily removed from the cavities because of the zero relief angles of the cavities. In total, 25 shots were made. CMM measurements on the deformation at the bottoms of the inserts showed that, up to 25 shots, the plastic deformation at the mould inserts A, C, and D was not discernible. The negligible deformation that occurred on these three inserts, indicated that insert D, made by the LBFF, had at least as much ability to resist deformation under pressure with 25 shots as did insert A, which was made of as-received 304 stainless steel. If the injected blocks can be removed easily from the inserts, injection moulding could be an effective way to examine the wear resistance of the mould inserts of different materials under given test conditions. In this study, there was no discernible effect on the mould inserts from the injected material owing to the low abrasive characteristics of the polystyrene used for injection and the small number of shots.

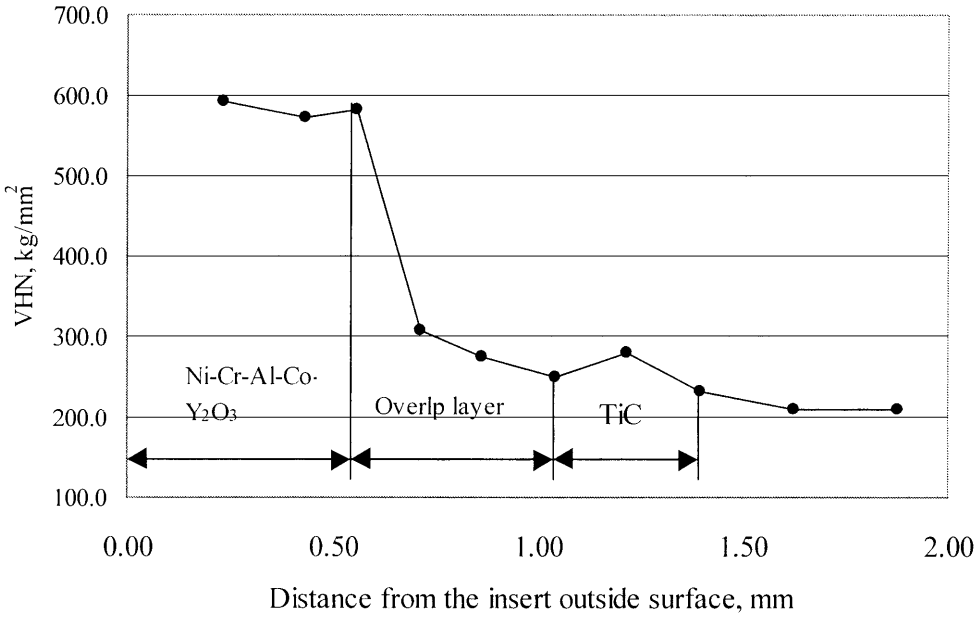

Fig. 10. Vickers microhardness variation with the distance from the insert surface.

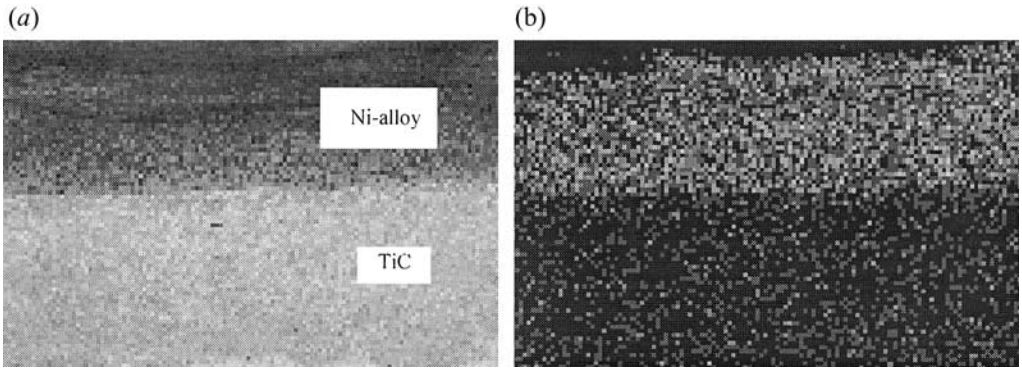

Fig. 11. (*a*) SEM micrograph and (*b*) carbon content variation.

Table 6. Classification of mould inserts for performance evaluation.

Mould insert	Materials	Surface microhardness, (kg mm^{-2})	Surface roughness (μm)	Evaluation tests
A	As-received 304 stainless steel	220	4.5	Injection moulding
B	Hardened H-13 die steel	570	1.0	Die casting, thermal fatigue
C	Laser-coated (TiC) 304 stainless steel	1400	20.0	Die casting, injection moulding, thermal fatigue
D	FGM (TiC+Ni-Cr-Al-Co-Y_2O_3)	583	10.0	Die casting, injection moulding, thermal fatigue

3.4.3 Low-Cycle Thermal Fatigue Test

For moulds used in the injection and die-casting processes, thermal fatigue is the most common failure mode owing to exposure of such parts to varying temperatures and stresses. Because thermal fatigue is related not only to the material and test conditions, but also to the specimen geometry, a temperature cycle may produce different stress cycles. For comparison, inserts B, C, and D were tested under the same test conditions and with the same geometry. The inserts were first subjected to temperature cycles in the range 20°C–650°C. Insert C had cracks on the TiC coating side when there were 10 cycles, whereas inserts B and D did not show any crack initiation up to 35 cycles. The early occurrence of cracks on insert C was expected because of pre-existing defects and possible residual stresses related to the processing of TiC and the lower fatigue

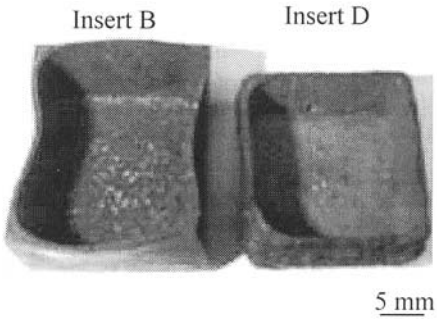

Fig. 12. The deformation of mould inserts after the thermal fatigue test.

strength of 304 stainless steel. Inserts B and D were then tested at temperature cycles of 20°C–960°C. At this elevated temperature, the onset of deformation of insert B was unexpectedly observed when there were 5 cycles; the deformation became more severe as the number of cycles increased (Fig. 12). Crack initiation occurred on insert B after 30 cycles. Although insert D had cracks in the TiC layer when the number of cycles was 17, it did not show any evidence of deformation (Fig. 12). In addition, more oxide scale was observed on insert B than on insert D, indicating that insert B was more susceptible to cyclic oxidation. Table 7 gives the results of low-cycle thermal fatigue tests. The significant differences in deformation behaviour between inserts B and D indicate that insert D has higher strength at elevated temperatures. The greater strength may be attributed to the presence of 0.5% Y_2O_3 in the Ni-alloy composite and to the laser processing. The existence of Y_2O_3 in the metal matrix acts to pin down the dislocation motion and extends the performance of the Ni-alloy. Laser processing can maintain the fine size of the dispersoids without agglomeration because of its ability to purify the Y_2O_3 particles and redistribute them more uniformly, because such particles absorb more laser energy than the surrounding matrix does [18]. The content of nickel and chromium, and the adhesion of the chromium oxide (Cr_2O_3) scale owing to the homogeneous distribution of the Y_2O_3 dispersoids, may explain why insert D has low susceptibility to cyclic oxidation [19]. Differences in crack patterns and thermal cycles between inserts B and D could be attributed to the differences in sensitivity to stresses and to the differences in ductility of the materials. The extended performance of insert D at elevated temperature can be useful in aluminium die-casting and plastic injection moulding.

Table 7. Thermal fatigue test results for mould inserts *B*, *C*, and *D*

Mould insert	Stage I*	Stage II†
B	35 cycles without any deformation and crack initiation	Deformation started at cycle 5 and cracks occurred at cycle 30
C	10 cycles with crack initiation	N/A
D	35 cycles without any deformation and crack initiation	No evidence of deformation. Crack initiation at cycle 17

*The inserts were alternatively immersed in a heated furnace of 650°C for 3 min and dropped in water at room temperature to finish one cycle. †The inserts were alternatively immersed in a heated furnace of 960°C for 2 min and dropped in water at room temperature to finish one cycle.

4. Conclusions

An LBFF process was successfully developed to build up overlapping layers, using TiC powder and Ni-Cr-Al-Co-Y_2O_3 composite powder. Based on the investigation of the fabricated inserts, the principal conclusions are as follows:

1. The process can be used to fabricate functional parts with any materials suitable for laser cladding.
2. The insets have a high surface hardness and have the expected toughness. These properties are suitable for mould and die applications.
3. The fabricated inserts have been tested functionally with the 319 aluminium casting process and the polystyrene injection moulding process; tests indicated that the inserts made by the LBFF process could be used for functional purposes with minimum post-processing.
4. Low-cycle thermal fatigue tests indicate that the laser-fabricated FGM insert has a higher strength and improved dimensional stability at elevated temperatures than the hardened H13 die steel insert. However, the thermal fatigue resistance of the hardened H13 die steel insert is slightly better than that of the laser-fabricated FGM insert. The high strength and dimensional stability of the FGM insert at elevated temperatures could be explained by the presence of 0.5% Y_2O_3 in the Ni-alloy composite and by the benefits of laser processing.

Acknowledgements

Many thanks are due to Larry Couture for providing the CNC machine and assisting in conducting the experiments.

References

1. http://www.modernmachineshop.com/articles/hsm9801.html, 2000.
2. K. Stoeckhert (ed.), Mold-Making Handbook for the Plastic Engineer, Hanser, Munich Vienna New York, 1983.
3. N. B. Dahotre (ed.), Laser in Surface Engineering, ASM International®, pp xiii–xvi, 1998.
4. J. Mazumder, J. Choi, K. Nagarathnam, J. Koch and D. Hetzner, "The direct metal deposition of H13 tool steel for 3-D components", Journal of Metals, pp. 55–60, May 1997.
5. R. Irving, "Taking a powder – metallurgy and lasers are cooking up new methods for manufacturing", Mechanical Engineering, pp. 55–59, September 1999.
6. G. K. Lewis, "Direct laser metal deposition process fabrication near-net-shape components rapidly", Materials Technology, 10, pp. 51–54, 1995.
7. J. O. Milewski, G. K. Lewis, D. J. Thoma, G. I. Keel, R. B. Nemec and R. A. Reinert, "Direct light fabrication of a solid metal hemisphere using 5-axis powder deposition", Journal of Materials Processing Technology, 75, pp. 165–172, 1998.
8. M. Binnard, Design by Composition for Rapid Prototyping, Kluwer, Boston, 1999.

9. D. H. Abbott and F. G. Arcella, "AeroMet implementing novel Ti process", Metal Powder Report, 53(2), pp. 24–26, 1998.
10. A. Ghosh, Y. Miyamoto, I. Reimanis and J. J. Lannutti (ed.), "Functionally graded materials: manufacture, properties, and application", American Ceramic Society, 76, pp. 171–174, 1997.
11. http://www.handyharmancanada.com/TheBrazingBook/comparis.htm, 2000.
12. J. D. Ayers, "Wear behavior of carbide-injected titanium and aluminum alloys", Wear, 97, pp. 249–266, 1984.
13. A. G. Grigoryants, Basics of Laser Material Processing, Mir, Moscow, 1994.
14. http://www.sulzermetco.com/products/material/mt_nick.html, 15 December, 2000.
15. J. Mazumder, O. Conde, R. Villar and W. Steen (ed.), Laser Processing: Surface Treatment and Film Deposition, Kluwer, 1996.
16. E. W. Kreutz, G. Backes, A. Gasser and K. Wissenbach, "Rapid prototyping with CO_2 laser radiation", Applied Surface Science, 86, pp. 310–316, 1995.
17. J. D. Ayers and T. R. Tucker, "Particulate-TiC-hardened steel surfaces by laser melt injection", Thin Solid Films, 73, pp. 210–207, 1980.
18. P. A. Molian, Y. M. Yang and P. C. Patnaik, "Laser Welding of Oxide Dispersion-Strengthened Alloy MA 754", Journal of Materials Science, 27, pp. 2687–2694, 1992.
19. G. H. Gessinger, Powder Metallurgy of Superalloys, Butterworth, 1984.